Solar Scattering from Condensation in Apollo Translunar Injection Plume

R. T. V. KUNG,* L. CIANCIOLO,* AND J. A. MYER†
Avco Everett Research Laboratory, Everett, Mass.

For the Translunar Injection burn of the Saturn IV B spacecraft during the Apollo 8 mission, a spectacular visible plume was photographed by the Smithsonian Astrophysical Observatory on Mt. Haleakela, Hawaii. The specific mechanism responsible for the plume radiance has not been unambiguously identified, although solar scattering from ice crystal formed in the expanding plume has been suggested as a plausible mechanism. In this work, we have calibrated and reduced the raw photographic data and have used nonrigorous condensation theory to predict ice particle condensation and size distributions. Our data reduction and analysis indicate that 5–10% condensation with particle sizes in the 70–100 Å range would be necessary to explain the observed data.

Nomenclature

$c(1)$ = water monomer concentration
c_N = particle number density
C = heat capacity
d = throat diameter
E = effective irradiance on film (joules/cm^2)
f = H_2O flow rate
$f\#$ = f number
g = percentage condensation
h = vehicle altitude
I_B = blackbody function
I_ξ = radiant intensity scattered per particle
J_n = nucleation rate (nuclei/cc × sec)
k = Boltzman constant
K = effective radiance (w/cm^2 × ster)
l = plume length
L_f = latent heat of sublimation
m = molecular mass
n = index of refraction
N = molecules per particle
P = pressure
P_∞ = flat surface vapor pressure of water
Q = radiant intensity (w/ster)
Q_{abs} = absorption cross section
r = radius of droplet
r^* = critical radius
R = gas constant
S = supersaturation ratio
t = flowfield time variable
t' = time referenced to J-2 ignition
Δt = exposure time
T = temperature
T_e = earth temperature (300 K)
u = flow velocity
v = vehicle velocity
x = flowfield distance variable
y = mole fraction of species
α = sticking coefficient
γ = specific heat ratio
Γ = adjustable parameter accounting for variation from Volmer's theory
ζ = Stefan-Boltzman constant
λ = wavelength
ν = collision frequency
ξ = angle subtended by the solar flux and the scattered radiation
ρ = molecular density
σ = surface tension of ice (96 dynes/cm)
τ = droplet residence lifetime
τ_e = telescope transmission
τ_a = atmospheric transmission
ϕ = number of collisions
χ = solar constant
ψ = stellar correction factor for absolute intensity

Subscripts

c = condensed phase or droplet
H = hydrogen
w = water vapor
o = stagnation conditions

I. Introduction

THE sequence of photographs shown in Fig. 1 are of the Translunar Injection (TLI) burn of the Saturn IV B spacecraft during the Apollo 8 mission on Dec. 21, 1968. They were recorded at the Smithsonian Astrophysical Observatory facility on Mt. Haleakela, Hawaii, using their 20″ f/1 Baker-Nunn satellite tracking camera. The Saturn IV B has a single Rocketdyne J-2 engine that develops 2×10^5 lb of thrust using a liquid H_2/O_2 fuel mixture. The TLI burn lasts for approximately a six-minute duration with engine ignition at 15:44′:37″ GMT and shutdown (352 sec later) at 15:50′:29″ GMT. Translated into HST, the event occurred roughly between 5:45 and 5:50 a.m. For this particular event, the trajectory and the position of the sun were so located that the spacecraft and plume were sun illuminated while the sky background was dark at the observation site. Under these conditions there was sufficient contrast so that the reflected or scattered visible sunlight from the Saturn IV B rocket body and plume was clearly observable from this position on the Earth.

The specific mechanism responsible for the plume radiance has not been unambiguously identified. However, there has been a general concensus[1,2] that it is due to sunlight scattered from the ice crystals formed by condensation in the rapidly expanding plume. The work described in this paper attempts to determine whether this proposed phenomenology is physically reasonable. With the raw SAO photographic data, the techniques of photographic photometry (with stellar photometric standards) was applied to determine the absolute intensity of the plume. Concurrently, we have used condensation theory on the J-2 engine flowfield in order to predict the particle size distribution, number density, and subsequent scattered radiation intensity. The signature estimates were then parameterized over the range of

Received May 10, 1974; revision received September 11, 1974. This work was supported by ARPA under Contract F04701-73-C-0284. The authors wish to express appreciation toward B. J. Wu of Yale University, for stimulating discussions, as well as the Smithsonian Astrophysical Observatory who kindly lent us the raw data film for reduction.

Index categories: Multiphase Flows; Rarefied Flows.

* Senior Scientist.
† Staff Scientist; presently at SAI, Inc., La Joya, Calif.

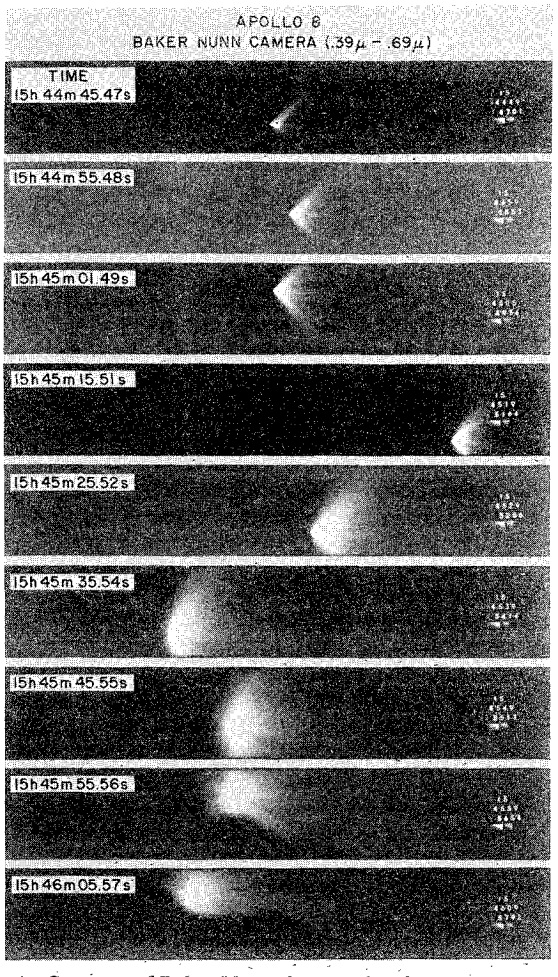

Fig. 1 Sequence of Baker-Nunn photographs of Apollo 8 TLI burn.

reasonable particle sizes and degrees of condensation and compared with the actual data.

II. Data Reduction

Three of the data frames shown in Fig. 1 were chosen to be photometrically reduced and used in the analysis. Enlargements of these three frames are shown in Fig. 2. They were recorded on 2475 film with 0.4 sec exposures at 18, 24, and 48 sec after engine ignition. During the period of open shutter, the moving Apollo vehicle and the plume produced a streaked film image. For frame number 2 at 45 m 1.49 s the camera was in siderial track mode; but for frames 1 and 3 at 44 m 55.48 s and 45 m 25.52 s both the stars and the Apollo were streaked. In spite of the fact that the telescope was supposedly tracking the vehicle in frames number 1 and 3, the resulting length of the streaked image of the SIV B vehicle itself in the 0.4 sec exposures is essentially the same for all three data frames. These three frames were chosen because a) they were from quite early times and the apparent size of the plumes appeared to correlate reasonably well with the predicted sizes, b) they were not in the saturation regime of film response, c) they were reasonably well contained within the telescope field-of-view and did not appear to be occulted by intervening clouds.

The data were reduced to absolute intensity in units of w/ster using the techniques of photographic photometry with stellar standards used for the absolute calibration. Similar data reduction techniques have been used with the same camera and film on several extended barium cloud sources of visible luminescence and the agreement obtained with other sensors in these cases gives us a high degree of confidence in the applicability of such techniques. The calibration techniques and data have been

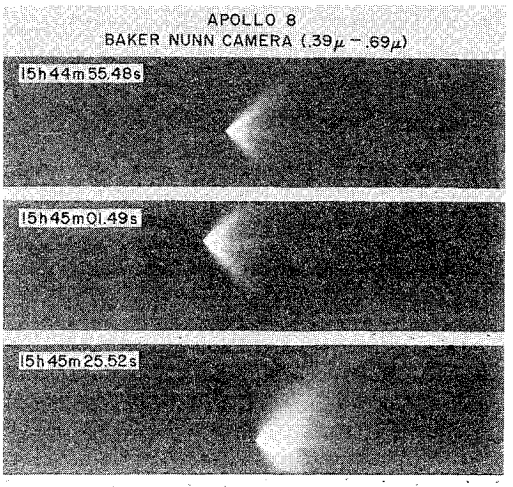

Fig. 2 Data frames calibrated and reduced.

extensively described elsewhere[3,4] and will thus only be briefly reviewed here.

The frames of Fig. 2 were densitometered and the density profile of the image converted to intensity. The use of "photometric standard" star images on each frame and a relative intensity scale obtained from a photographic step wedge produced an absolute calibration of intensity.

The relationship used to obtain radiance distribution at the plume is:

$$K = (4/\pi)[(f\#)^2 E\psi/\tau_e \tau_a \Delta t] \quad (1)$$

With an extended source of radiation the objective of the data reduction is to obtain the intensity of an equivalent point source which is equal to the integrated intensity over the extended source. The density profiles for the data frames were converted to radiance and numerically integrated to obtain radiant intensity. The area or spatial extent of the plume was determined from its angular extent and slant range. The slant range was determined from a knowledge of the vehicle altitude (h) and its position in the background star field. The pertinent data frames are listed in Table 1.

Table 1 Summary of Apollo data

	t' (sec)	h (km)	v (m/sec)	Az (°)[a]	Plume length (km)
1)	18	175.9	~7500	153	11
2)	24	175.9	~7500	148	15
3)	48	175.8	~7700	124	30

[a] Azimuthal angle.

The total integrated intensity for each of the three frames is plotted as a function of time in Fig. 3. An error bar is included for the data from frame 2. This very large error bar is a reflection of the fact that only one visible standard star could be observed in the field of view of this particular frame. Frames 1 and 3 had at least 3 observable stellar standards within the field of view resulting in a substantial reduction of the uncertainty in determining the value of ψ for these frames.

III. Mechanisms

As was mentioned in Sec. I, the current observations were obtained in what is commonly referred to as "the twilight window." That is when the vehicle in its trajectory above the Earth is sunlit, while the sky background at the observation station is essentially dark.

Other Apollo series TLI's have occurred with similar trajectories over the same section of the Earth. These have, however, occurred under either full daylight or night time conditions

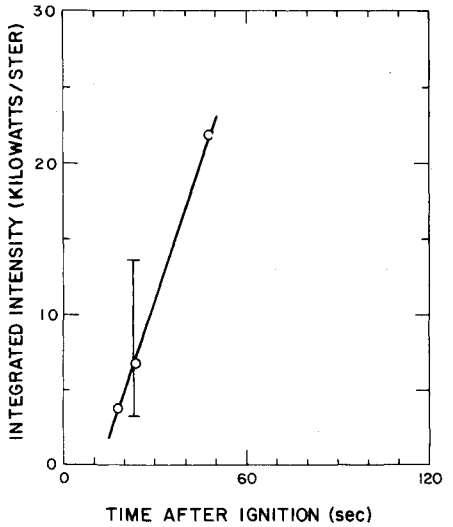

Fig. 3 Total integrated intensity of Apollo 8 TLI plume ($\Delta\lambda$ 0.39–0.69 μ) as a function of time.

over Hawaii. For the night time conditions no visible plumes have been observed. It is thus apparent that the observed luminescence can only be observed with dark sky conditions and must be caused by a mechanism that is solar stimulated. Otherwise, a series of such spectacular events could not have occurred undetected for the previous night time TLI's.

Since it is a solar-triggered mechanism, this effectively rules out mechanisms which are solar independent. These include the more common mechanisms of a) atomic or molecular flame fluorescence, b) chemiluminescence (i.e., $A+B \rightarrow AB+h\nu$), c) radiative attachment (i.e., $X+e \rightarrow X^- + h\nu$), which are common sources of visible luminescence. The two most promising mechanisms that can be considered are a) the scattering of solar visible radiation from particles or droplets formed by condensation in the rapidly expanding plume flowfield, and b) resonance fluorescence from flowfield atomic or molecular species.

To assess the resonance fluorescence mechanism, a knowledge of the species that are present in the flowfield is required. Table 2 lists the species and their relative mole fractions that have been predicted to be present in the J-2 exhaust. These species calculations have been performed for the engine exit plane composition using the AERL "finite rate chemistry nozzle calculation." This calculation includes, a one-dimensional isentropic equilibrium expansion from combustion chamber conditions to a short distance beyond the throat as well as a one-dimensional finite-rate chemistry calculation of conditions throughout the divergent portion of the nozzle in order to determine the flow properties and species concentrations at the exit plane. It has been assumed that beyond the exit plane there are few enough collisions so that the chemistry can be essentially treated as frozen.

An assessment of the species listed in Table 2 reveals that none of these species possess strong electronic transitions in the visible region of the spectrum. It thus appears that resonance fluorescence of any major flowfield species can be ruled out as a possible mechanism. There is also the possibility that resonance fluorescence from atomic impurities (sodium for example) present in small amounts in the flowfield could be a source of visible radiation. However, the fact that the observed radiation was reported to be "white light"[5] with no dominant hue probably rules out atomic impurities since the resonantly scattered radiation from atomic species would be expected to have a dominant color characteristic of the observed electronic transitions.

Table 2 Apollo exit plane composition

Species	Mole fraction
H	1.6×10^{-3}
OH	8.7×10^{-5}
H_2	0.31
H_2O	0.69
O	4.1×10^{-7}
O_2	9×10^{-7}
HO_2	7×10^{-10}
Impurities	?

We are thus left with the apparent conclusion (as was mentioned in Sec. I) that this phenomenon has to be due to sunlight scattering from ice crystals formed by condensation in the rapidly expanding plume. In the following sections we will attempt to ascertain whether or not this hypothesis is physically reasonable.

IV. Analysis

A. Particle Formation

In an attempt to examine whether or not the ice particle formation hypothesis is physically reasonable, classical nucleation theory of Volmer will be applied to the present problem, in addition to correlation with available molecular beam experimental results.

The theory in its various forms has been reviewed by Wegener and Parlange,[6] and will not be derived here. It is important to point out that the classical nucleation theory is a steady-state theory valid for constant temperature and pressures. In a free jet expansion, however, there are large temperature gradients. This perturbation causes rigorous application of this theory questionable. Because of the lack of a more appropriate theory, we propose to use Volmer's theory as a first approximation in estimating the number of nuclei formed in the expanding jet.

The governing equation for the rate of nucleation[7,8] under constant temperature and pressure conditions is

$$J_n = \Gamma \frac{c(1)}{\rho_c}\left(\frac{2\sigma m}{\pi}\right)^{1/2} c(1)\exp\left(-\frac{4\pi r^{*2}\sigma}{3kT}\right) \tag{2}$$

where

$$r^* = 2\sigma m/\rho_c kT \ln S \tag{3}$$

is the critical radius.

During the clustering process, latent heat is released heating the nuclei to a higher temperature than the ambient gas. If large amounts of inert gas were present, the clusters can be quickly equilibrated with the ambient gas. This is the condition under which Eq. (2) holds. Under the Apollo plume conditions where the main constituents are 70% H_2O and 30% H_2, the possible lack of complete thermal equilibration will impede the condensation process. Feder, et al.[9] derived the following correction factor for the nucleation rate including finite heat transfer,

$$J_{\text{non-is}} = (b^2/b^2+q^2) \times J_n \tag{4}$$

where b^2 is the mean square of the energy fluctuation of the impinging molecules, and q^2 involves the latent heat released and surface free energy change resulting from the addition of a monomer. For the Apollo case, Wu[10] calculated a value of $\sim 10^{-2}$ for this correction factor.

Depending on the various forms of the homogeneous nucleation theory, the value of Γ can range between 1 and 10^{14}. Various values of Γ predict onset of nucleation at different regions of an expanding flow where the supersaturation ratio S required to yield an appreciable nucleation rate would be drastically different. Since the supersaturation ratio increases exponentially as the temperature decreases, it is thus a strong function of the distance parameter in the flowfield. This results in the insensitivity of the onset region to the uncertainty in Γ. In addition, subsequent growth of nuclei far downstream of the onset is little affected by this uncertainty. Nucleation onset can be conveniently defined by 0.1% condensation. With the estimated uncertainty in Γ, Wu calculated the nucleation onset zone to be between 40 and 50 m downstream of the exit plane for the center streamline, and a nuclei concentration of approximately 10^{10} nuclei/cc, with a critical radius of 3 to 4 Å. The nucleation zones for two different

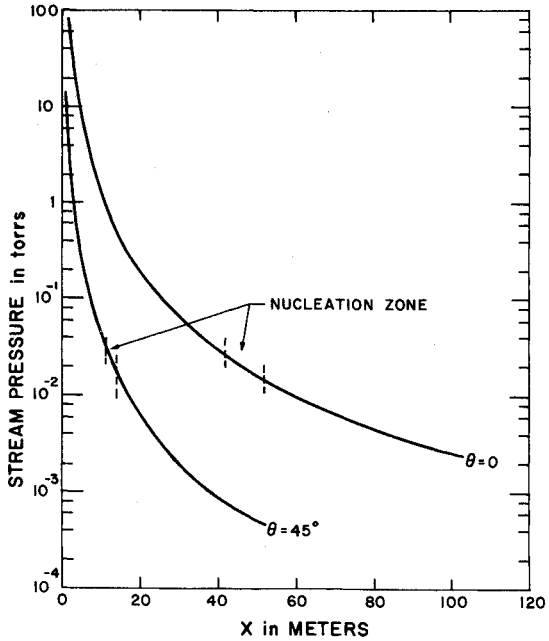

Fig. 4 Nucleation zones for 0° and 45° streamlines.

streamlines are shown in Fig. 4. Figure 5 gives the nucleation zones as a function of local temperature.

The rate of growth of the nucleated particles is given by[8]

$$\frac{dr}{dt} = \alpha \frac{m}{\rho_c}\left[\frac{P - P_c}{(2\pi mkT)^{1/2}}\right] \tag{5}$$

where P_c is given by the Thomson equation[11]:

$$P_c = P_\infty \exp(2\sigma m/\rho_c kT_c r) \tag{6}$$

The measured sticking coefficient of H_2O molecules on ice[12] in the temperature range between 133 K and 158 K is 0.83 ± 0.15. At condensation onset, $P = P_c$. Since the flow is expanding, P quickly becomes greater than P_c, in which case particle growth will proceed at a rate of the order of 40 Å/*ms* or equivalently 10 Å/m as calculated from Eq. (5) and the local stream conditions. Droplet growth is limited by a maximum temperature increase of 50 K (see Fig. 5), beyond which the saturation vapor pressure of the droplets becomes greater than the ambient water

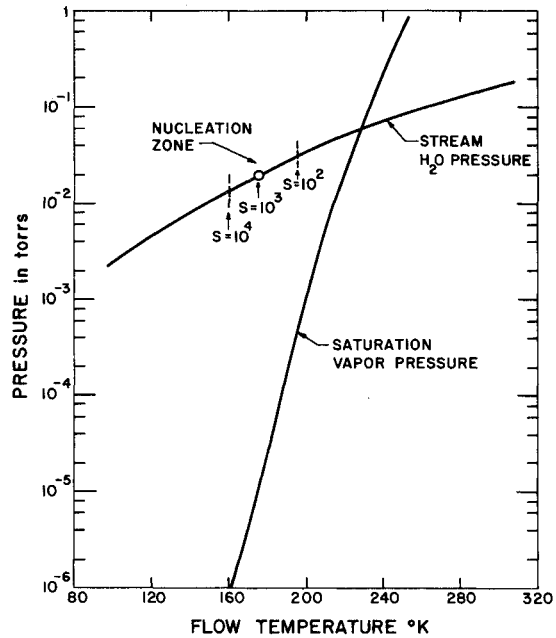

Fig. 5 Nucleation zones as a function of local temperature.

vapor pressure. By assuming that the droplet temperature equilibrates with the ambient gas temperature, an estimate to the percentage allowable condensation g is easily calculated from the following energy conservation equation:

$$L_f g y_w = [g y_w C_c + (1-g) y_w C_w + y_H C_H + R]\Delta T \tag{7}$$

For $\Delta T = 50$ K as obtained from Fig. 5, g is $\sim 5\%$. Table 3 lists for 5% condensation the particle radii r, corresponding to various particle number densities C_N, and the number of monomers per particle, N. Particle radii of 15 Å to 71 Å are possible for the given constraints. Further cooling along the expanding stream-tubes may allow for continued growth.

Table 3 Particle sizes for 5% condensation

C_N (particle/cc)	N (molecules/particle)	r (Å)
10^9	5×10^4	71 Å
10^{10}	5×10^3	33 Å
11^{11}	5×10^2	15 Å

In view of the recent molecular beam experiment of Stein and Armstrong[13] on the condensation of H_2O and CO_2, it is appropriate to apply Hagena and Obert's[14] scaling law to the present problem. This approach may have better validity than the theory. This scaling law is experimentally derived, thus nonequilibrium effects are inherently included within the experimental range of conditions. In a separate experiment, Golomb, et al.,[15] have substantiated this scaling law. The Hagena and Obert results indicate that for a given nozzle diameter and final cluster size, the stagnation condition scales as $P_o T_o^{(1.25\gamma - 0.5)/(1-\gamma)} = \text{const}$. In addition, for a given T_o and final cluster size, the nozzle diameter scales as $P_o d^a = \text{const}$, where $a = 0.8$ and 0.6, respectively, for inert gases and CO_2. Using a similar approach as Oman and Calia[16] in which the corresponding states argument was invoked, the same scaling law would hold for CO_2 and H_2O. Stein and Armstrong's conditions ($P_o = 5300$ mm *Hg*, $T_o = 441$ K, $d = 0.028$ cm, and $N = 2600$ molecules/cluster) can be applied to yield $P_o T_o^{-3.55} = 2.2 \times 10^{-6}$ mm $\times$ K$^{-3.55}$ for $\gamma = 1.33$. Extrapolating to the Apollo stagnation temperature of 3390 K, an equivalent $P_o = 7.5 \times 10^6$ mm *Hg* and $P_o d^{0.6} = 8.8 \times 10^5$ mm $\times$ cm$^{0.6}$ corresponding to $N = 2600$ molecules/cluster are obtained. Using the actual Apollo conditions of $T_o = 3390$ K, $P_o(H_2O) = 2.4 \times 10^4$ mm *Hg* and an equivalent sonic nozzle diam of 93 cm [obtained from Eq. (7′) of Hagena and Obert with an actual throat diam of 37 cm] results in $P_o d^{0.6} = 3.6 \times 10^5$ mm $\times$ cm$^{0.6}$. Oman and Calia pointed out that in correlating particle sizes, the relationship $N \propto (P_o d^{0.6})^{3.5}$, which holds for CO_2, is applicable. The result of this intercorrelation yields a particle size of ~ 100 molecules/particle ($r \simeq 9$ Å) for the Apollo case. Stein and Armstrong obtained their results at a position of $x/d = 39.2$ downstream of the nozzle. To estimate the equivalent flow regime in which this correlation has been made, the following Sherman and Ashkenas[17] T vs x relationship can be applied, by assuming that initial nucleation process has not appreciably altered the flowfield.

$$\frac{T}{T_o} \approx \frac{2}{(\gamma-1)G^2}\left(\frac{x}{d}\right)^{2-2\gamma} \tag{8}$$

For $\gamma = 1.33$, G is ~ 3.8. The calculated ratio of T/T_o is ~ 0.037 in Stein and Armstrong's experiment. The implication is that the condensation has proceeded to ~ 100 molecules/cluster at a temperature of 125 K (for $T_o = 3390$ K), or equivalently at approximately 80 m downstream of the exit. This result is consistent with Wu's calculation that onset occurs at ~ 170 K with a critical radius of ~ 4 Å at ~ 40 m downstream of the exit. It is wise to caution that this type of correlation is extremely sensitive to the uncertainty in the stagnation temperature. In fact, the cluster size is sensitive to approximately the 7th power of T_o. Scaling beyond the experimental range may be invalid as was cautioned by Hagena and Obert.

Oman and Calia, without the benefit of Stein and Armstrong's

experiment, used the principle of corresponding states between N_2, CO_2, and H_2O and scaled the Apollo case to obtain a particle radius of 90 Å at approximately 10 to 30 m downstream of the exit for the center streamline. In the light of Stein and Armstrong's experiment, this estimate is most likely inaccurate. In addition, classical nucleation theory predicts negligible condensation in this flow regime.

In highly underexpanded jets, it is very likely that the rate controlling step in the condensation is termolecular dimer formation, in which event, the governing correlation is $P_o d^{0.5} =$ const.[18] The number of termolecular collisions encountered by a single water molecule in expanding from 300 K is estimated in the Appendix to be $\sim\frac{1}{2}$ collision. For a local flow density of $\sim 2\times 10^{15}$ molecules/cc, the total number of triple collisions is $\sim 1\times 10^{15}$. Smith[19] calculated an efficiency of 1 in 44 collisions for the iodine atom recombination with Xe as the third body. There is no reason to expect the same efficiency for H_2O dimer formation. But it is not unreasonable to assume an efficiency of 10^{-5} to 10^{-6}, in which case 10^9 to 10^{10} dimers/cc could be formed between 300 K and 200 K in the flow. Magnusson[20] measured an equilibrium const of 3.6×10^{-21} cc/molecule for $(H_2O)_2$ in CCl_4 solutions at 293 K. Viktorova and Zhevakin[21] calculated a value of 6.8×10^{-21} cc/molecule for this constant at 298 K. Under equilibrium conditions, the dimer concentration in the plume at $\sim$300 K is $\sim 5\times 10^9$ molecules/cc. It is not unreasonable to conceive that 10^9 to 10^{10} dimers can be formed during the expansion. These dimers would then take the role of nucleation sites for further bimolecular growth.

B. Particle Light Scattering

With the theoretical discussion as a background, an expression for the amount of solar visible radiation scattered per spherical ice crystal as a function of radius will be derived. The radiant intensity scattered per particle (I_ξ) for $2\pi r/\lambda < 1$ is given by the Rayleigh equation[22]:

$$I_\xi = 8\pi^4 r^6(1+\cos^2\xi)\left|\frac{n^2-1}{n^2+2}\right|^2 \frac{\int(1/\lambda^4)I_B(\lambda)\,d\lambda}{\int I_B(\lambda)\,d\lambda}\chi \qquad (9)$$

where ξ is assumed to be 90°, and $n = 1.33$ at visible wavelengths. Using the equivalent sunlight temperature of 5800 K at the upper atmosphere, the ratio of the integrals is 2.1×10^{17} cm^{-4}. With a value of 0.04 w/cm^2 for the solar constant in the 0.39 to 0.69 μ visible region results in

$$I_\xi = 5.6\times 10^{17}\, r^6 \text{ w/ster} \times \text{particle}$$

The total number of single size particles in the plume is given by

$$\Sigma = glf/uN \qquad (10)$$

With $l = 13$ km, $f = 7.7\times 10^{27}$ H_2O/sec, and $u = 4.2\times 10^5$ cm/sec, the total radiant intensity (Q) is simply $\Sigma \times I_\xi$ for the optically thin plume. Table 4 lists a range of particle sizes, number density, and calculated radiant intensities. Particle sizes of 70–100 Å at 5–10% condensation can explain the listed experimental observation (under Table 4) quite reasonably, where the comparison should be made with frame 1.

Table 4 Calculated radiant intensity[a]

r(Å)	N (monomers/particle)	C_N (#/cc)	g (% condensation)	Σ	Q (w/ster)
7	50	10^{12}	0.05	2×10^{25}	1.4
15	500	10^{11}	0.05	2×10^{24}	1.4×10^1
33	5000	10^{10}	0.05	2×10^{23}	1.4×10^2
71	5×10^4	10^9	0.05	2×10^{22}	1.4×10^3
19	10^3	10^{11}	0.1	2×10^{24}	5.7×10^1
42	10^4	10^{10}	0.1	2×10^{23}	5.7×10^2
89	10^5	10^9	0.1	2×10^{22}	5.7×10^3
193	10^6	10^8	0.1	2×10^{21}	5.7×10^4

[a] Q photo: frame 1 = 3.76×10^3 (t' = 18 sec); frame 2 = 6.76×10^5 (t' = 24 sec); frame 3 = 2.18×10^4 (t' = 48 sec).

C. Particle Residence Time

There are principally two mechanisms by which monomers can evaporate from clusters in a very low density ambient gas. One mechanism is due to the fluctuation of the distribution of internal energy. However, as long as the cluster temperature is below 150 K, droplets will evaporate at less than 1 Å/sec. In addition, this process is self-arresting. The other mechanism is heating due to earthshine. An upper bound to the rate of change of particle size through earthshine heating can be estimated by the following relationship:

$$L_f(dN/dt) = -4\pi r^2 Q_{abs}\zeta T_e^4 \qquad (11)$$

where it is assumed that all energy absorbed ends up in the latent heat of sublimation. Other heat transfer mechanisms have been neglected, such as thermal equilibration with the surrounding gases. The absorption coefficient (Q_{abs}) is taken to be independent of wavelength. These assumptions will yield a lower bound to the lifetime for the largest value of Q_{abs}. Equation (11) reduces to

$$\frac{dr}{dt} = -\frac{m}{\rho_c}\frac{Q_{abs}\zeta T_e^4}{2L_f} \qquad (12)$$

where

$$Q_{abs} = \text{Real}\left\{i\left(\frac{8\pi r}{\lambda}\frac{(n^2-1)}{(n^2+2)}\right)\right\} \qquad (13)$$

for $2\pi r/\lambda < 1$. Table 5 lists the indices of refraction of ice at two wavelengths.[23]

Table 5 Indices of refraction of H_2O

λ	n
6.1 μ	$1.234 - i\,0.0643$
3.08 μ	$1.225 - i\,0.3428$

The largest value of Q_{abs} (at $\lambda = 3.08$ μ) is

$$Q_{abs} = 1.7\times 10^4\, r \qquad (14)$$

Substitution of Eq. (14) into (12) with appropriate constants yields

$$dr/dt = -0.142\, r \qquad (15)$$

or $\tau \sim 7$ sec.

Similarly, for the 6.1 μ absorption band, τ is $\sim$80 sec. The actual lifetime is greater than the values calculated. The long residence time of particles can explain the fact that frame 3 gives 10 times larger radiant intensity than frame 1.

V. Discussion

In an attempt to interpret the plume radiance from Apollo 8 TLI, we have made an estimate on the ice crystal sizes and number densities formed in the plume. From the thermodynamic point of view, classical nucleation theory was used to estimate the number density of nuclei produced in the flow. The rate of growth of particles and nonisothermal effects were taken into account in a nonrigorous fashion. Correlation with molecular beam experiments were carried out reinforcing the possibility of nuclei formation. From the microscopic viewpoint, it was shown that the likely rate controlling termolecular recombination reaction is physically realizable.

Particle sizes of 70 Å–100 Å at 5%–10% condensation are necessary to explain the data. These are not physically unreasonable requirements in view of the nucleation theory and kinetics of particle growth.

An interesting and yet unresolved problem revolves around the evidence that larger angle streamlines indicated more light scattering than smaller angle streamlines. Molecules in the outer streamlines have shorter transit times which suggests less likelihood in achieving condensation, in contradiction to the observation. In an attempt to examine this phenomenon, a characteristic calculation taking account of freestream impact pressure was performed. The outer streamlines may pass through

a weak diffuse barrel shock at high altitude which could conceivably serve to enhance the molecular and particle collision frequency, thus facilitating condensation. However, no indication of pressure rise was evident from the calculation. In addition, classical theory and Hagena and Obert's scaling law (where the equivalent nozzle diameter is smaller for the outer streamlines), both predict less condensation in the outer streamlines. However, it is conceivable, that if termolecular reactions are rate controlling, the outer streamlines would have less nuclei formed, but the bimolecular growth process could allow the fewer nuclei to grow to larger sizes. A comparison of particle sizes with $r = 33$ Å at 5% condensation and $r = 89$ Å at 1% condensation yields the ratio $Q(r = 89\ \text{Å})/Q(r = 33\ \text{Å}) \sim 4$. This reveals that for larger sizes and less condensation, it is possible to have larger scattered intensity.

Another possible mechanism in explaining the anomaly may be due to ambient oxygen atoms ($\sim 10^{10}$/cc at 100 to 200 km) initiating heterogeneous nucleation in the outer streamlines. No experimental data are available for direct comparison with the Apollo conditions. Experiments simulating these conditions can be of extreme importance in elucidating this nonsteady process and in interpreting rigorously the Apollo data.

Comment Added in Proof

It was suggested that unburnt liquid fuel and/or oxidizer along the walls may serve as nucleation sites. A close-circuit cooling system maintains the J-2 nozzle wall temperature to $\geqq 500$ K.[26] This excludes the possible existence of unburnt liquid during the TLI.

Appendix: Thermolecular Collisions

The thermolecular collision frequency encountered by a single molecule is[15,24]

$$\nu = B\tfrac{2}{3}\pi^2\sigma_a{}^5\left(\frac{3kT}{\pi m}\right)^{1/2}\rho^2 \tag{A1}$$

where $B \simeq 4$, is a geometric factor. $\sigma_a = 2.71$ Å.[25] The number of collisions is given by

$$\phi = \int \nu\, dt \tag{A2}$$

Differentiating Eq. (8), yields

$$\frac{dT}{dx} = -\frac{4}{d}\left(\frac{\gamma-1}{2}\right)^{(2\gamma-1)/(2\gamma-2)}(A)^{1/(\gamma-1)}T\left(\frac{T}{T_o}\right)^{1/(2\gamma-2)} \tag{A3}$$

The flow velocity is given by

$$\frac{dx}{dt} \approx \left(\frac{\gamma}{\gamma-1}\right)^{1/2}\left(\frac{kT_o}{m}\right)^{1/2} \tag{A4}$$

Putting Eqs. (A1), (A3), and (A4) into Eq. (A2) together with the isentropic relationship, yields

$$N_c = -H\rho_o{}^2(1/T_o)^{(4-\gamma)/(2\gamma-2)}\left[T_2{}^{(4-\gamma)/(2\gamma-2)} - T_1{}^{(4-\gamma)/(2\gamma-2)}\right] \tag{A5}$$

where

$$H = B\tfrac{2}{3}\pi^2\sigma_a{}^5\left(\frac{3}{\pi}\right)^{1/2}\left(\frac{\gamma-1}{\gamma}\right)^{1/2}\frac{d}{4}\left(\frac{\gamma-1}{2}\right)^{-(2\gamma-1)/(2\gamma-2)}A^{-1/(\gamma-1)} \tag{A6}$$

Evaluating this expression, yields $H = 10^{-35}$ cm^6. For $\rho_o = 3\times 10^{19}$ molecules/cc, $T_1 = 300$ K and $T_2 = 200$ K, ϕ is 0.5 collision.

References

[1] Vaughan, O. H., Jr., "Analysis of Apollo 8 Photography and Visual Observation," SP 201, 1969, pp. 92–102, NASA.

[2] Lundquist, C. A., "Photometry from Apollo Tracking," *Space Research X*, edited by T. M. Donahue, P. A. Smith, and L. Thomas, North-Holland Publishing Co., Amsterdam, 1970, pp. 25–32.

[3] Cianciolo, L., Myer, J. A., and Kivel, B., "Avco Everett Data Report for Operation Birdseed," ARPA Order No. 1443, Oct. 1970, Avco Everett Research Lab., Everett, Mass.

[4] Cianciolo, L., Myer, J. A., and Kivel, B., "Avco Everett Data Report for Operation Barbizon," ARPA Order No. 1443, July 1972, Avco Everett Research Lab., Everett, Mass.

[5] Perry, W., private communication, Smithsonian Astrophysical Observatory, Mt. Haleakala, Hawaii, 1972.

[6] Wegener, P. P. and Parlange, J. Y., "Condensation by Homogeneous Nucleation in the Vapor Phase," *Naturwissenschaften*, Vol. 57, No. 11, Nov. 1970, pp. 525–533.

[7] Volmer, M., *Kinetik der Phasenbildung*, Dreden-Leipzig, Steinkopff, 1939.

[8] Hill, P. G., Witting, H., and Demetri, E. P., "Condensation of Metal Vapors During Rapid Expansion," *ASME Transactions Journal of Heat Transfer*, Ser. C., Vol. 85, Nov. 1963, pp. 303–317.

[9] Feder, J., Russell, K. C., Lothe, J., and Pound, G. M., "Homogeneous Nucleation and Growth of Droplets in Vapors," *Advances in Physics*, Vol. 15, 1966, pp. 111–178.

[10] Wu, C. B., "Possible Condensation in Rocket Exhaust Plume," ARPA Order No. 1179, April 1973, Yale University, New Haven, Conn.

[11] Frenkel, J., *Kinetic Theory of Liquids*, Oxford, New York, 1946, p. 368.

[12] Koros, R. M., "Sticking Probability of Water Vapor Molecules on an Ice Surface," Doctoral Thesis, Chemical Engineering Dept., Princeton University, N.J., 1961.

[13] Stein, G. D. and Armstrong, J. A., "Structure of Water and Carbon Dioxide Clusters Formed via Homogeneous Nucleation in Nozzle Beams," *Journal of Chemical Physics*, Vol. 58, No. 5, March 1973, p. 1999–2003.

[14] Hagena, O. F. and Obert, W., "Cluster Formation in Expanding Supersonic Jets: Effect of Pressure, Temperature, Nozzle Size, and Test Gas," *Journal of Chemical Physics*, Vol. 56, March 1972, pp. 1793–1802.

[15] Golomb, D., Good, R. E., Bailey, A. B., Busby, M. R., and Dawbarn, R., "Dimer, Clusters and Condensation in Free Jets. II," *Journal of Chemical Physics*, Vol. 57, Nov. 1972, pp. 3844–3853.

[16] Oman, R. A. and Calia, V. S., "Non-Equilibrium Cluster Formation in Rocket Exhausts," RM-571, March 1973, Grumman Aerospace Corp., Bethpage, N.Y.

[17] Ashkenas, H. and Sherman, F. S., "Structure and Utilization of Supersonic Free Jets in Low Density Wind Tunnels," *Rarefied Gas Dynamics*, 4th Symposium, Institute for Aerospace Studies, University of Toronto, Canada, Vol. 2, 1965, pp. 84–105.

[18] Milne, T. A., Vandegrift, A. G., and Green, F. T., "Mass-Spectrometric Observations of Argon Clusters in Nozzle Beams II. The Kinetics of Dimer Growth," *Journal of Chemical Physics*, Vol. 52, No. 3, Feb. 1970, pp. 1552–1560.

[19] Smith, F. T., "Three-Body Collision Rates in Atomic Recombination Reactions," *Discussion of the Faraday Society*, Vol. 33, 1962, pp. 183–188.

[20] Magnusson, L. B., "Infrared Absorbance by Water Dimer in Carbon Tetrachloride Solution," *Journal of Physical Chemistry*, Vol. 74, No. 24, Nov. 1970, pp. 4221–4228.

[21] Viktorova, A. A. and Zhevakin, S. A., "The Water-Vapor Dimer and its Spectrum," *Soviet Physics—Daklady*, Vol. 11, No. 12, June 1967, pp. 1059–1062.

[22] Van de Hulst, H. C., *Light Scattering by Small Particles*, Wiley, New York, 1957.

[23] Irvine, W. M. and Pollack, J. B., "Infrared Optical Properties of Water and Ice Spheres," *ICARUS*, Vol. 8, 1968, pp. 324–360.

[24] Benson, S. W., *Chemical Kinetics*, McGraw-Hill, New York, 1969, p. 169.

[25] Monchick, L. and Mason, E. A., "Transport Properties of Polar Gases," *Journal of Chemical Physics*, Vol. 35, No. 5, Nov. 1961, pp. 1676–1697.

[26] Campbell, D., private communication, Rocketdyne, Inc., Canoga Park, Calif., 1974.